

Kinetic Energy Distribution of Fragments for Thermal Neutron-Induced ^{235}U and ^{239}Pu Fission Reactions*

Xiaojun Sun^{1,†}, Haiyuan Peng¹, Liying Xie¹, Kai Zhang¹, Yan Liang¹,
Yinlu Han^{1,2}, Nengchuan Shu², Jie Yan³, Jun Xiao³, and Junjie Sun³

¹*College of Physics, Guangxi Normal University, Guilin 541004, People's Republic of China*

²*China Institute of Atomic Energy, P. O. Box 275(41), Beijing 102413, People's Republic of China and*

³*Institute of Nuclear Physics and Chemistry, China Academy of Engineering Physics, Mianyang 621900, People's Republic of China*

(Dated: February 12, 2021)

The Dinuclear and Statistical Model (DSM), which focuses on the generation and evolution of vast complementary pairs of the primary fission fragments at the scission moment, is proposed. (1) The fissile nucleus is assumed to elongate along a symmetric coaxial until it breaks into two primary fission fragments. (2) Every complementary pair of the primary fission fragments is approximately described as two ellipsoids with large deformation. (3) The kinetic energy in the pair is mainly provided by the Coulomb repulsion, which is explicitly expressed through strict six-dimensional integrals. (4) Only three phenomenological coefficients are obtained to globally describe the quadrupole deformation parameters of arbitrary primary fragments both for $^{235}\text{U}(n_{th}, f)$ and $^{239}\text{Pu}(n_{th}, f)$ reactions, based on the common characteristics of the measured data, such as mass and charge distributions, kinetic energy distributions. In the framework of DSM, the explicit average total kinetic energy distribution $\overline{TKE}(A)$ and the average kinetic energy distribution $\overline{KE}(A)$ are consistently represented. The theoretical results in this paper agree well with the experimental data. Furthermore, the reliable DSM is expected to generally evaluate the corresponding observables for thermal neutron-induced fission of actinides.

I. INTRODUCTION

Nuclear fission has exceptionally challenged the theoretical research since its discovery in the late 1930s [1]. The evolution of a nucleus from a compact configuration into two separated fragments is an intricate puzzle [2], featuring not only the collective movement of large-scale nucleons, but also the various structural effects. The current theoretical descriptions of fission reflect the complexity and richness revealed in experimental studies, emphasizing the multidimensional, dynamic, and microscopic aspects [3]. Despite tremendous advances in theory, there is not yet a quantitative theory of fission [3]. This is unfortunate because nuclear fission remains important to the society due to its practical applications, in safeguards, accelerator technology, homeland security, medicine, energy production, and waste transmutation at nuclear reactors [4–6], and r -process in the merging of neutron stars [7, 8].

The majority of energy released in neutron-induced fission of actinides is in the form of kinetic energy in the fission fragments [9]. This kinetic energy is measured by experiments and generally expressed in the relationship with the mass number A of the light and heavy fragments of the average total kinetic energy distribution $\overline{TKE}(A)$

and the average kinetic energy distribution $\overline{KE}(A)$. As an important part of the observables, it has a close relationship with other observables (such as mass distribution, charge distribution, neutron multiplicity, and so on). Moreover, it is closely related to shell effect [10], which is helpful for the research of nuclear structure.

It is universally acknowledged that the transformation of fissile nucleus from a single system to two systems is one of the critical problems. Therefore, a comprehensive description of the deformation of these large primary fragments is indispensable to quantitatively predict the fission products. Some macroscopic models, macroscopic and microscopic models, microscopic models, and time-dependent microscopic theories [11–17] have been used to calculate deformation parameters from fissile nucleus to fission fragments. Albeit the well-established physics of these models, the calculated results of fission products vary greatly, with obscure problems concerning the microscopic fission theory. For example, the dissipation coefficient in the fission process is difficult to be calculated by the microscopic method. The evolution relationship between quantum tunneling effect and dissipation effect, and the coupling of different dimensional degrees of freedom in multi-dimensional fission, are necessary to be further considered. It is widely shared that the results of these microscopic models have not yet been adopted by the latest evaluation nuclear data libraries, such as ENDF/B-VIII.0 [18], JEFF-3.3.1 [19], JENDL-4.0u2 [20], CENDL-3.1 [21], and so on.

Machine learning method developed in recent years plays a very important role in the evaluation of nuclear data [22, 23]. It optimizes the theoretical data and the accuracy, but ignores some physical evolution processes.

* This work is supported by National Natural Science Foundations of China (No. 12065003, 12042508, 11465005); Natural Science Foundation of Guangxi (No. 2019GXNSFDA185011) and Key Laboratory of Neutron Physics China Academy of Engineering Physics (No. 2018BA03).

† sxj0212@gxnu.edu.cn

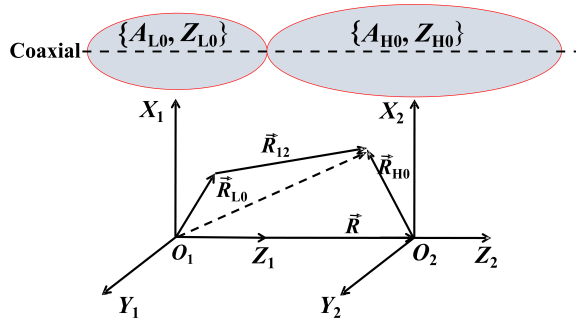


FIG. 1. The schematic of dinuclear and coordinate system at the scission moment.

The semi-empirical GEF model [2] summarizes the fundamental laws of physics and the general properties of microscopic systems and mathematical objects. Many fission observables can be more accurately calculated with no need to specifically adjust the measurement and empirical data of a single system. This unique feature, which is of great value in evaluating nuclear data, is difficult to account for the fission process. The pre-scission configuration (PSC) approach represents that the part of the neck will be incorporated into the nascent light and heavy fragments at the scission moments. So the electrostatic interactions between a rotational ellipsoid and a sphere, and between two ellipsoids, are employed to describe the kinetic energy. This approach can provide trust enough $\overline{TK\overline{E}}(A)$ distributions and extend the fissioning systems for which experimental $\overline{TK\overline{E}}(A)$ data do not exist [24].

In this paper, a new DSM is proposed to concurrently calculate $\overline{TK\overline{E}}(A)$ and $\overline{KE}(A)$ of fragments for thermal neutron-induced ^{235}U and ^{239}Pu fission reactions. In section II, The derivation process of the Coulomb repulsion is introduced in detail. In section III, the deformation parameters of the primary fragments at the scission moment are generally described. The calculated results and analyses are shown in section IV. And simple conclusions are given in section V.

II. COULOMB REPULSION

It is widely shared that the fissile nucleus $\{Z_f, A_f\}$ elongates along the symmetric coaxial because of the deformation energy. With its elongation to a certain degree, the fissile nucleus will attain the scission point and split into a multitude of complementary fission fragment pairs $\{Z_{L0}, A_{L0}; Z_{H0}, A_{H0}\}$ [25], which are unstable neutron-rich nuclei and hold large kinetic energy under the Coulomb repulsion. Furthermore, they de-excite through emitting fast neutrons and γ photons, and evolve to initial fission products $\{Z_{L0}, A_L; Z_{H0}, A_H\}$, which will further de-excite through emitting slow neutrons and β

ray to form relatively stable secondary fission products $\{Z_L, A_L; Z_H, A_H\}$.

Complementary primary fragments have complex shapes at the scission moment. Although the expression for the Coulomb interaction of two deformed, arbitrarily oriented, axially symmetric nuclei is obtained [26], it is difficult to derive the analytical formula. To vividly describe the fissile system at the scission point, the dinuclear concept is used in this paper. If the fissile nucleus is assumed to stretch along the symmetric coaxial until it breaks into two primary fission fragments, every complementary pair of the primary fission fragments is approximately described by two ellipsoids with large deformation at the scission moment. The schematic of dinuclear and coordinate systems at the scission point is shown in Fig. 1. The kinetic energy in every complementary pair of the primary fragments is mainly provided by the Coulomb repulsion, with the representation of the Coulomb interaction shown as follows [26]:

$$V_C = e^2 \int \frac{\rho_{L0}(\vec{R}_{L0}) \rho_{H0}(\vec{R}_{H0})}{|\vec{R}_{12}|} d\vec{R}_{L0} d\vec{R}_{H0}, \quad (1)$$

the amount of e^2 in Eq. (1) is a charge constant with a value of 1.44 MeV·fm. The distance \vec{R}_{12} between $d\vec{R}_{L0}$ and $d\vec{R}_{H0}$ for the primary fission fragment pairs can be obtained from Fig. 1 as

$$\vec{R}_{12} = \vec{R} + \vec{R}_{H0} - \vec{R}_{L0}. \quad (2)$$

The denominator [26, 27] in Eq. (1) is

$$\begin{aligned} \frac{1}{|\vec{R}_{12}|} &= \sum_{l_{L0}, l_{H0}=0}^{\infty} \frac{R_{L0}^{l_{L0}} R_{H0}^{l_{H0}}}{R^{l_{L0}+l_{H0}+1}} \\ &\times \frac{4\pi(-1)^{l_{L0}}(l_{L0}+l_{H0})!}{\sqrt{(2l_{L0}+1)(2l_{H0}+1)}} \\ &\times \sum_m \frac{Y_{l_{L0}m}(\theta_{L0}, \varphi_{L0})}{\sqrt{(l_{L0}+m)!(l_{L0}-m)!}} \\ &\times \frac{Y_{l_{H0}m}(\theta_{H0}, \varphi_{H0})}{(l_{H0}+m)!(l_{H0}-m)!}. \end{aligned} \quad (3)$$

Where $Y_{lm}(\theta, \varphi)$ is a spherical harmonic function, and $R_{L0}, R_{H0}, \theta_{L0}, \varphi_{L0}, \theta_{H0}, \varphi_{H0}$ are the spherical coordinates in the laboratory coordinate systems O_1 and O_2 , respectively.

The numerators $\rho_{L0}(\vec{R}_{L0})$ and $\rho_{H0}(\vec{R}_{H0})$ in Eq. (1) are the proton density in the light and heavy primary fragments, respectively. Because of the high excited energy of the primary fragments, the proton distribution is assumed to be uniform in their ranges $R_i(\theta_i)$ ($i = L0$ or $H0$ which denotes the light and heavy primary fragments, as the same in the next text if specifically unmarked). So in this paper, a homogeneous charged drop with a sharp surface is adopted, with its proton density is expressed

as

$$\rho_i(\vec{r}) = \begin{cases} \rho_i & 0 \leq r \leq R_i(\theta_i) \\ 0 & r \geq R_i(\theta_i). \end{cases} \quad (4)$$

$R_i(\theta_i)$ defines the distance from the origin of the coordinate system to the point on the nuclear surface. For an axially deformed system, $R_i(\theta_i)$ is expressed as

$$R_i(\theta_i) = R_i [1 + \beta_i Y_{lm}(\theta_i)], \quad (5)$$

where $R_i = r_0 A_i^{1/3}$, $r_0 = 1.226$ fm [28]. β_i is a quadrupole deformation parameter, which is very important to describe the tensile strength of the primary fragments [17]. So the distance between the centers of mass of light and heavy primary fragments can be rewritten as

$$R = R_{L0} [1 + \beta_{L0} Y_{20}(0)] + R_{H0} [1 + \beta_{H0} Y_{20}(\pi)]. \quad (6)$$

In order to obtain the explicit form of the Coulomb repulsion V_C expressed in Eq. (1) for different complementary fragment pairs, the charge densities should be firstly calculated through the definition of proton number, i.e. $Z_i = \int \rho_i(\vec{r}) d\vec{r}$. Thus, the expression of the light and heavy kernel densities can be represented as

$$\rho_i = \frac{3Z_i}{4\pi R_i^3 (1 + \frac{12}{5} B_i^2 + \frac{16}{35} B_i^3)}, \quad (7)$$

where $B_i = \sqrt{5}\beta_i/\sqrt{16\pi}$.

Eq. (1) requires a six-dimensional integral, which can be firstly rewritten as:

$$V_C = e^2 \int \rho_{L0}(\vec{R}_{L0}) d\vec{R}_{L0} Q_1. \quad (8)$$

Where, Q_1 can be represented as:

$$Q_1 = \int_0^{2\pi} \int_0^\pi \sin \theta_{H0} d\theta_{H0} d\varphi_{H0} \times \int_0^{R_{H0}(\theta_{H0})} \rho_{H0} \frac{1}{|\vec{R}_{12}|} R_{H0}^2 dR_{H0}. \quad (9)$$

The spherical harmonic function $Y_{lm}(\theta, \varphi)$ can be expanded as

$$Y_{lm}(\theta, \varphi) = \sqrt{\frac{(2l+1)(l-m)!}{4\pi(l+m)!}} P_{lm}(\cos \theta) e^{im\varphi}. \quad (10)$$

If $m \neq 0$, $\int_0^{2\pi} e^{im\varphi} d\varphi = 0$, Eq. (10) is meaningless. Conversely, if $m = 0$, $\int_0^{2\pi} e^{im\varphi} d\varphi = 2\pi$, Q_1 can be expressed as:

$$Q_1 = \sqrt{\pi} \rho_{H0} \sum_{l_{L0}=0}^{\infty} \frac{4\pi(-1)^{l_{L0}} R_{L0}^{l_{L0}} Y_{l_{L0},0}(\theta_{L0}, \varphi_{L0})}{l_{L0}! R_{L0}^{l_{L0}+1} \sqrt{2l_{L0}+1}} \times \int_{-1}^1 \sum_{l_{H0}=0}^{\infty} \frac{(l_{L0}+l_{H0})! R_{H0}^{l_{H0}+3}}{l_{H0}! R_{H0}^{l_{H0}+3}} \times (1 - B_{H0} + 3B_{H0}x_1^2)^{l_{H0}+3} P_{l_{H0}}(x_1) dx_1, \quad (11)$$

where $x_1 = \cos \theta_{H0}$ and $x_1 \in [-1, 1]$.

Obviously, the integral and summation can be exchanged. Thus, Q_1 can be rewritten as

$$Q_1 = \sqrt{\pi} \rho_{H0} \sum_{l_{L0}=0}^{\infty} \frac{4\pi(-1)^{l_{L0}} R_{L0}^{l_{L0}} Y_{l_{L0},0}(\theta_{L0}, \varphi_{L0})}{l_{L0}! R_{L0}^{l_{L0}+1} \sqrt{2l_{L0}+1}} \times [l_{L0}! p_0 + (l_{L0}+2)! p_2 + (L_{L0}+4)! p_4 + (l_{L0}+6)! p_6 + \dots]. \quad (12)$$

While $l_{H0} = 0, 2, 4, 6$, and p_0, p_2, p_4, p_6 are expressed as follows

$$\begin{aligned} p_0 &= \frac{R_{H0}^3}{3} (2 + \frac{24}{5} B_{H0}^2 + \frac{32}{35} B_{H0}^3), \\ p_2 &= \frac{R_{H0}^5}{10R^2} (4B_{H0} + \frac{32}{7} B_{H0}^2 + \frac{96}{7} B_{H0}^3 \\ &\quad + \frac{640}{77} B_{H0}^4 + \frac{3392}{1001} B_{H0}^5), \\ p_4 &= \frac{R_{H0}^7}{168R^4} (\frac{48}{5} B_{H0}^2 + \frac{192}{11} B_{H0}^3 + \frac{6528}{143} B_{H0}^4 \\ &\quad + \frac{6144}{143} B_{H0}^5 + \frac{5376}{187} B_{H0}^6 + \frac{334848}{46189} B_{H0}^6), \\ p_6 &= \frac{R_{H0}^9}{6480R^6} (\frac{3456}{143} B_{H0}^3 + \frac{41472}{715} B_{H0}^4 \\ &\quad + \frac{373248}{2431} B_{H0}^5 + \frac{8736768}{46189} B_{H0}^6 \\ &\quad + \frac{7796736}{46189} B_{H0}^7 + \frac{85598208}{1062347} B_{H0}^8 \\ &\quad + \frac{467361792}{26558675} B_{H0}^9). \end{aligned} \quad (13)$$

By substituting Eqs. (12) and (13) into Eq. (8), V_C can be rewritten as:

$$V_C = e^2 \rho_{L0} \rho_{H0} \sqrt{\pi} Q_2. \quad (14)$$

Where Q_2 can be expressed as:

$$Q_2 = \sqrt{\pi} \int_{-1}^1 \sum_{l_{L0}=0}^{\infty} \frac{4\pi(-1)^{l_{L0}} R_{L0}^{l_{L0}+3}}{(l_{L0}+3)l_{L0}! R_{L0}^{l_{L0}+1}} \times [l_{L0}! p_0 + (l_{L0}+2)! p_2 + (l_{L0}+4)! p_4 + (l_{L0}+6)! p_6 + \dots] (1 - B_{L0} + 3B_{L0}x_2^2)^{l_{L0}+3} \times P_{l_{L0}}(x_2) dx_2. \quad (15)$$

Where $x_2 = \cos \theta_{L0}$ and $x_2 \in [-1, 1]$.

As same as Q_1 , Q_2 can be rewritten as:

$$Q_2 = \sqrt{\pi} (s_0 + s_2 + s_4 + s_6 + \dots). \quad (16)$$

While $l_{L0} = 0, 2, 4, 6$, s_0, s_2, s_4, s_6 are expressed as fol-

laws:

$$\begin{aligned}
s_0 &= \frac{4\pi R_{L0}^3}{3R} (p_0 + 2!p_2 + 4!p_4 + 6!p_6 + \dots) \\
&\quad \times \left(2 + \frac{24}{5}B_{L0}^2 + \frac{32}{35}B_{L0}^3\right), \\
s_2 &= \frac{4\pi R_{L0}^5}{3R} \frac{3R_{L0}}{10R^2} (2!p_0 + 4!p_2 + 6!p_4 + 8!p_6 + \dots) \\
&\quad \times \left(4B_{L0} + \frac{32}{7}B_{L0}^2 + \frac{96}{7}B_{L0}^3 + \frac{640}{77}B_{L0}^4\right. \\
&\quad \left.+ \frac{3392}{1001}B_{L0}^5\right), \\
s_4 &= \frac{4\pi R_{L0}^3}{3R} \frac{3R_{L0}^4}{168R^4} (4!p_0 + 6!p_2 + 8!p_4 \\
&\quad + 10!p_6 + \dots) \left(\frac{48}{5}B_{L0}^2 + \frac{192}{11}B_{L0}^3 + \frac{6528}{143}B_{L0}^4\right. \\
&\quad \left.+ \frac{6144}{143}B_{L0}^5 + \frac{5376}{187}B_{L0}^6 + \frac{334848}{46189}B_{L0}^7\right), \\
s_6 &= \frac{4\pi R_{L0}^3}{3R} \frac{3R_{L0}^6}{6480R^6} (6!p_0 + 8!p_2 + 10!p_4 \\
&\quad + 12!p_6 + \dots) \left(\frac{3456}{143}B_{L0}^3 + \frac{41472}{715}B_{L0}^4\right. \\
&\quad \left.+ \frac{373248}{2431}B_{L0}^5 + \frac{8736768}{46189}B_{L0}^6 + \frac{7796736}{46189}B_{L0}^7\right. \\
&\quad \left.+ \frac{85598208}{1062347}B_{L0}^8 + \frac{467361792}{26558675}B_{L0}^9\right).
\end{aligned} \tag{17}$$

After sorting out and omitting the higher order terms, the explicit Coulomb repulsion can be obtained:

$$\begin{aligned}
V_C &= \frac{e^2 Z_{L0} Z_{H0}}{R f_0(B_{L0}) f_0(B_{H0})} \{ [f_0(B_{H0}) \\
&\quad + 2!f_2(B_{H0}, R_{H0}) + 4!f_4(B_{H0}, R_{H0})] f_0(B_{L0}) \\
&\quad + [2!f_0(B_{H0}) + 4!f_2(B_{H0}, R_{H0}) \\
&\quad + 6!f_4(B_{H0}, R_{H0})] f_2(B_{L0}, R_{L0}) \\
&\quad + [4!f_0(B_{H0}) + 6!f_2(B_{H0}, R_{H0}) \\
&\quad + 8!f_4(B_{H0}, R_{H0})] f_4(B_{L0}, R_{L0}) \}.
\end{aligned} \tag{18}$$

Where the compact forms of f function are listed as follows:

$$\begin{aligned}
f_0(x) &= 1 + \frac{12}{5}x^2 + \frac{16}{35}x^3, \\
f_2(x, y) &= \frac{3y^2}{10R^2} \left(2x + \frac{16}{7}x^2 + \frac{48}{7}x^3\right. \\
&\quad \left.+ \frac{320}{77}x^4 + \frac{1696}{1001}x^5\right), \\
f_4(x, y) &= \frac{3y^4}{168R^4} \left(\frac{24}{5}x^2 + \frac{96}{11}x^3 + \frac{3264}{143}x^4\right. \\
&\quad \left.+ \frac{3072}{143}x^5 + \frac{2688}{187}x^6 + \frac{167424}{46189}x^7\right).
\end{aligned} \tag{19}$$

Thus, the total kinetic energy of every complementary primary fragment pair can be rewritten as:

$$TKE = V_C(A_{L0}, Z_{L0}, \beta_{L0}; A_{H0}, Z_{H0}, \beta_{H0}). \tag{20}$$

And the average total kinetic energy of the complementary primary fragment pairs is expressed as:

$$\begin{aligned}
\overline{TKE}(A) &= \frac{1}{\sum_k} \sum_k TKE(A_{L0}(j), Z_{L0}(j, k), \\
&\quad \beta_{L0}(j, k); A_{H0}(j), Z_{H0}(j, k), \\
&\quad \beta_{H0}(j, k)),
\end{aligned} \tag{21}$$

where j denotes the number of the primary fragment pairs, and k denotes the isobar numbers of the j -th primary fragment pair.

From the Eqs. (18) - (21), the deformation parameters $\beta_{L0, H0}$ can be seen indispensable. However, it is impossible that these parameters can be experimentally and theoretically derived from in an accurate way. So in this paper, these quantities are obtained by the following methods in the next sections.

III. DEFORMATION PARAMETERS

A. Most Probable Primary Fragment Pair

It is widely shared that the primary fragment pairs at the scission moment must follow the laws:

$$\begin{aligned}
Z_f &= Z_{L0} + Z_{H0}, \\
A_f &= A_{L0} + A_{H0}.
\end{aligned} \tag{22}$$

In addition, the neutron separation energy of every primary fragment must hold the positive value, i.e., $S_n(Z_i, A_i) > 0$. Furthermore, the neutron-proton ratio of every possible primary fragment is larger than that of the fissile nucleus and the corresponding beta-decay stable nuclei. Thus, all of the possible primary fragment pairs can be predicted, as shown in Figs. 2 and 3 for $^{235}\text{U}(n_{th}, f)$ and $^{239}\text{Pu}(n_{th}, f)$ reactions, respectively. In these two figures, the gray points denote the measured mass nuclei compiled in AME2016 [29], while the black points denote the stable nuclei located in the vicinity of the beta stable line and the blue hollow points indicate the possible primary fragments predicted in this paper. Obviously, there are hundreds of possible primary fragment pairs $\{A_{L0}(j), Z_{L0}(j, k); A_{H0}(j), Z_{H0}(j, k)\}$, where j denotes the sequence number of the primary fragment pairs, and k labels the sequence number of the isobar pairs for the j -th primary fragment pair. From Figs. 2 and 3, slight discrepancies can be seen at the positions of the symmetrical fission points $\{A_f/2, Z_f/2\}$ for $^{235}\text{U}(n_{th}, f)$ and $^{239}\text{Pu}(n_{th}, f)$ reactions, respectively. And the total primary fragment amount of $^{239}\text{Pu}(n_{th}, f)$ reaction is a bit fewer than that of $^{235}\text{U}(n_{th}, f)$ reaction, which is slightly unexpected because the fissile nucleus with larger mass are generally believed to produce more primary fragments.

Theoretically, each primary fragment pair has different contribution to the kinetic energy. However, $\overline{TKE}(A)$ and $\overline{KE}(A)$ for fission reactions are only the functions

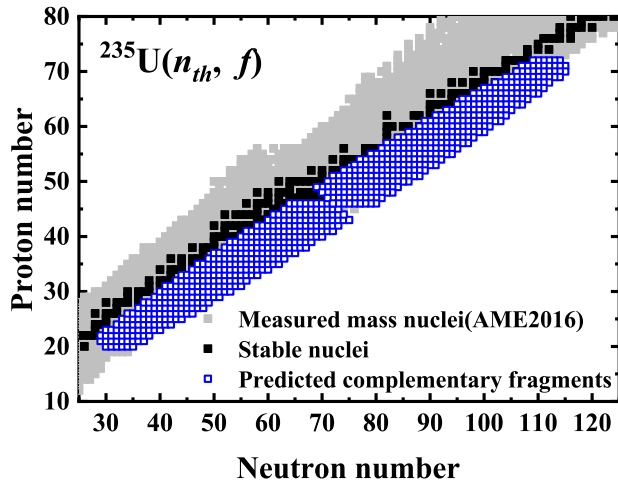


FIG. 2. (Color online) Possible primary fragment distribution for $^{235}\text{U}(n_{th}, f)$ fission reaction.

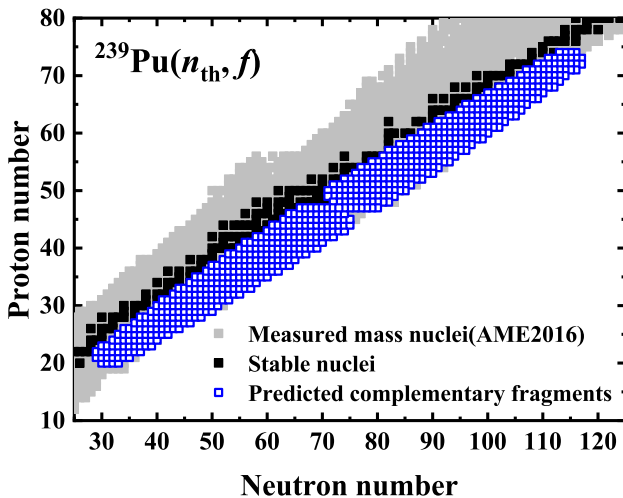


FIG. 3. (Color online) The same as Fig. 2 but for $^{239}\text{Pu}(n_{th}, f)$ reaction.

of the mass number. How to describe the partial contributions of each isobar pairs to the same fragment mass number A is one of the critical problems. To solve it, the common characteristics of the deformation for the vast primary fragments must be revealed. In this paper, it is assumed that only a pair of isobar, named after Most Probable Primary Fragment Pair, dominates the contributions to the same mass number A of the primary fragment, and the excited energies of the primary fragments are not high because of the large deformation energies at the scission moment. Thus, the Most Probable Primary Fragment Pairs can be selected on the basis of the characteristics of the ground state (such as half-life) of the primary fragment pairs.

Tables I and II partially list the possible primary fragment pairs and their half-lives in the ground states for

TABLE I. Partial possible primary fragment pairs and their half-lives in the ground states for $^{235}\text{U}(n_{th}, f)$ fission reaction. The experimental data are taken from IAEA - Nuclear Data Section [30]. Herein, units such as s, ms, min, h, d and y denote second, millisecond, minute, hour, day and year, respectively.

j	k	$A_{L0}(j)$	$Z_{L0}(j, k)$	$A_{H0}(j)$	$Z_{H0}(j, k)$	τ_{L0}	τ_{H0}
1	1	118	46	118	46	1.9s	1.9s
1	2	118	45	118	47	266ms	3.76s
1	3	118	44	118	48	99ms	2.69min
1	4	118	43	118	49	30ms	5s
2	1	117	46	119	46	4.3s	0.92s
2	2	117	45	119	47	0.44s	2.1s
2	3	117	44	119	48	151ms	2.69min
2	4	117	43	119	49	44.5ms	2.4min
3	1	116	46	120	46	11.8s	0.492s
3	2	116	45	120	47	0.68s	1.23s
3	3	116	44	120	48	204ms	50.8s
3	4	116	43	120	49	57ms	3.08s
4	1	115	46	121	46	25s	0.285s
4	2	115	45	121	47	0.99s	0.78s
4	3	115	44	121	48	0.318s	13.5s
4	4	115	43	121	49	78ms	23.1s
4	5	115	42	121	50	45.5ms	27.03h
5	1	114	46	122	46	2.42min	0.108s
5	2	114	45	122	47	1.85s	0.529s
5	3	114	44	122	48	0.54s	5.24s
5	4	114	43	122	49	0.1s	6.17s
5	5	114	42	122	50	58ms	Stable
6	1	113	46	123	46	93s	0.108s
6	2	113	45	123	47	2.8s	0.298s
6	3	113	44	123	48	0.8s	2.1s
6	4	113	43	123	49	0.152s	6.17s
6	5	113	42	123	50	80ms	129.2d
6	6	113	41	123	51	32ms	Stable
7	1	112	46	124	46	21.04h	38ms
7	2	112	45	124	47	3.6s	0.191s
7	3	112	44	124	48	1.75s	1.25s
7	4	112	43	124	49	0.271s	3.12s
7	5	112	42	124	50	0.12s	Stable
7	6	112	41	124	51	33ms	60.2d
8	1	111	46	125	46	23.4min	57ms
8	2	111	45	125	47	11s	0.159s
8	3	111	44	125	48	2.12s	0.68s
8	4	111	43	125	49	0.29s	2.36s
8	5	111	42	125	50	0.186s	9.64d
8	6	111	41	125	51	54ms	2.76y
9	1	110	46	126	46	Stable	48.6ms
9	2	110	45	126	47	3.35s	0.052s
9	3	110	44	126	48	12.04s	0.515s
9	4	110	43	126	49	0.9s	1.53s
9	5	110	42	126	50	0.296s	2.3×10^5 y
9	6	110	41	126	51	0.082s	12.35d
9	7	110	40	126	52	37.5ms	Stable
10	1	109	45	127	47	80.8s	0.109s
10	2	109	44	127	48	34.4s	0.37s
10	3	109	43	127	49	0.91s	1.09s
10	4	109	42	127	50	0.61s	2.1h
10	5	109	41	127	51	0.108s	3.85d
10	6	109	40	127	52	0.056s	9.35h

TABLE II. Partial possible primary fragment pairs and their half-lives in the ground states for $^{239}\text{Pu}(n_{th}, f)$ reaction.

j	k	$A_{L0}(j)$	$Z_{L0}(j, k)$	$A_{H0}(j)$	$Z_{H0}(j, k)$	τ_{L0}	τ_{H0}
1	1	120	47	120	47	1.23s	1.23s
1	2	120	46	120	48	492ms	50.8s
1	3	120	45	120	49	132ms	3.08s
2	1	119	47	121	47	2.1s	0.78s
2	2	119	46	121	48	0.92s	13.5s
2	3	119	45	121	49	171ms	23.1s
2	4	119	44	121	50	69.5ms	27.03h
3	1	118	47	122	47	3.76s	0.529s
3	2	118	46	122	48	1.9s	5.24s
3	3	118	45	122	49	266ms	1.5s
3	4	118	44	122	50	99ms	Stable
4	1	117	47	123	47	72.8s	0.298s
4	2	117	46	123	48	4.3s	2.1s
4	3	117	45	123	49	0.44s	6.17s
4	4	117	44	123	50	151ms	129.2d
4	4	117	43	123	51	44.5ms	Stable
5	1	116	47	124	47	230s	191ms
5	2	116	46	124	48	11.8s	1.25s
5	3	116	45	124	49	0.68s	3.12s
5	4	116	44	124	50	204ms	Stable
5	5	116	43	124	51	57ms	60.2d
6	1	115	47	125	47	20.0min	159ms
6	2	115	46	125	48	25s	0.68s
6	3	115	45	125	49	0.99s	2.36s
5	4	115	44	125	50	318ms	9.64d
6	5	115	43	125	51	78ms	2.75856y
7	1	114	47	126	47	4.6s	52ms
7	2	114	46	126	48	2.42min	0.515s
7	3	114	45	126	49	1.85s	1.53s
7	4	114	44	126	50	0.54s	2.3×10^5 y
7	5	114	43	126	51	100ms	12.35d
7	6	114	42	126	52	58ms	Stable
8	1	113	47	127	47	5.37h	109ms
8	2	113	46	127	48	93s	0.37s
8	3	113	45	127	49	2.8s	1.09s
8	4	113	44	127	50	0.8s	2.1h
8	5	113	43	127	51	152ms	3.85d
8	6	113	42	127	52	80ms	9.35h
9	1	112	46	128	48	21.04h	0.28s
9	2	112	45	128	49	3.6s	0.84s
9	3	112	44	128	50	1.75s	59.07min
9	4	112	43	128	51	271ms	9.05h
9	5	112	42	128	52	120ms	7.7×10^2 y
10	1	111	46	129	48	23.4min	154ms
10	2	111	45	129	49	11s	611ms
10	3	111	44	129	50	2.12s	2.23min
10	4	111	43	129	51	290ms	4.366h
10	5	111	42	129	52	186ms	69.6min
10	6	111	41	129	53	54ms	1.57×10^7 y

$^{235}\text{U}(n_{th}, f)$ and $^{239}\text{Pu}(n_{th}, f)$ reactions, respectively. The experimental data are taken from IAEA - Nuclear Data Section [30], with the first column denoting the j -th primary fragment pair, the second column labeling the k -th isobar pair of the j -th primary fragment pair, and the last two columns indicating the half-lives of the light and heavy primary fragments, respectively. Herein, the units

such as s, ms, min, h, d and y, denote second, millisecond, minute, hour, day and year, respectively. From tables I and II, the half-lives of the light and heavy primary fragments can be seen to exhibit large discrepancies. In this paper, the isobar pairs with the smallest values $\tau_{L0} + \tau_{H0}$ are assumed to be the candidates of the Most Probable Primary Fragment Pairs, all of which are listed in Tables III and IV for $^{235}\text{U}(n_{th}, f)$ and $^{239}\text{Pu}(n_{th}, f)$ reactions, respectively. It is worth mentioning that there are several isobar pairs, which values $\tau_{L0} + \tau_{H0}$ are roughly equal for some primary fragment pairs. Therefore, the isobar pairs with the smallest values of $|\tau_{L0} - \tau_{H0}|$ are empirically selected as the candidates of the Most Probable Primary Fragment Pairs.

B. Deformation Parameter

It is widely acknowledged that the shapes of the primary fragments at the scission moment are hardly obtained not only by the measurements but also by the theories. In order to obtain the general descriptions of the deformation parameters of the primary fragment pairs, average total kinetic energies are assumed to be only provided by the Most Probable Primary Fragment Pairs, and the effects of the excited energies on the deformation parameters are ignored at the scission moment because of the large deformation energies. Therefore, it is presumed that the deformation parameters of the primary fragments are dependent on the isospin asymmetry degree I , and can be expressed as:

$$\beta_i = \alpha_i I_i, \quad (23)$$

where α_i is the phenomenological parameter, and $I_i = (N_i - Z_i)/A_i$ ($i = L0$ or $H0$).

By substituting Eq. (23) into Eq. (21), the relationship between the mass number A and the phenomenological parameter α_i can be obtained, as shown in Figs. 4 and 5, from which the same slopes of the isotopes are seen as the blue lines in the range $A \geq 140$, and $A \leq A_f - 140$ with negative slopes. And in the residual region, the phenomenological parameter α_i is approximately viewed as the smooth single-valued function of the mass number A . The critical point $A = 140$ is exactly corresponded to the peaks of the measured mass distributions of the heavy fragments for low energy neutron-induced fission of actinides [31–36].

A large amount of the measured average total kinetic energy distributions, such as ^{231}Pa , ^{232}U , ^{233}U , ^{235}U , ^{237}Np , ^{239}Pu , ^{241}Pu , ^{241}Am and ^{243}Am induced by thermal neutrons, show that they peak at $A \approx 132$ [31–33, 37, 38, 40, 41]. And many measured charge distributions show that they peak at $Z \approx 54$ [42–44]. It is widely acknowledged that $A \approx 132$ and $Z \approx 54$ are closely related to the shell structure. It is inspired that $A \approx 132, 140, A_f/2$ and $Z \approx 54, Z_f/2$ are some crucial values for the average total kinetic energy distributions

TABLE III. The properties of the Most Probable Primary Fragment Pairs for $^{235}\text{U}(n_{th}, f)$ reaction. β_i, α_i and I_i denote the quadrupole deformation parameter, phenomenological parameter and the isospin asymmetry degree, respectively.

A_{L0}	Z_{L0}	β_{L0}	α_{L0}	I_{L0}	A_{H0}	Z_{H0}	β_{H0}	α_{H0}	I_{H0}
118	46	1.3445	6.1020	0.2203	118	46	1.3445	6.1020	0.2203
117	45	1.3796	5.9782	0.2308	119	47	1.2559	5.9782	0.2101
116	45	1.3147	5.8658	0.2241	120	47	1.2709	5.8658	0.2167
115	45	1.2599	5.7955	0.2174	121	47	1.2932	5.7955	0.2231
114	45	1.1506	5.4652	0.2105	122	47	1.2543	5.4652	0.2295
113	45	1.0701	5.2574	0.2035	123	47	1.2395	5.2574	0.2358
112	44	1.0736	5.0099	0.2143	124	48	1.1313	5.0099	0.2258
111	43	0.9958	4.8058	0.2072	125	48	1.1149	4.8058	0.2320
110	43	0.9881	4.5287	0.2182	126	49	1.0064	4.5287	0.2222
109	43	0.9204	4.3618	0.2110	127	49	0.9960	4.3618	0.2283
108	43	0.8575	4.2094	0.2037	128	49	0.9866	4.2094	0.2344
107	43	0.8157	4.1561	0.1963	129	49	0.9987	4.1561	0.2403
106	43	0.7882	4.1777	0.1887	130	49	1.0284	4.1777	0.2462
105	42	0.8241	4.1205	0.2000	131	50	0.9751	4.1205	0.2366
104	42	0.7968	4.1435	0.1923	132	50	1.0045	4.1435	0.2424
103	42	0.7778	4.2166	0.1845	133	50	1.0462	4.2166	0.2481
102	41	0.8281	4.2231	0.1961	134	51	1.0085	4.2231	0.2388
101	41	0.8226	4.3727	0.1881	135	51	1.0689	4.3727	0.2444
100	41	0.8214	4.5633	0.1800	136	51	1.1408	4.5633	0.2500
99	40	0.8834	4.6031	0.1919	137	52	1.1088	4.6031	0.2409
98	41	0.7938	4.8619	0.1633	138	51	1.2683	4.8619	0.2609
97	39	0.9181	4.6870	0.1959	139	53	1.1127	4.6870	0.2374
96	39	0.9086	4.8460	0.1875	140	53	1.1769	4.8460	0.2429
95	38	0.9673	4.8368	0.2000	141	54	1.1320	4.8368	0.2340
94	37	1.0198	4.7930	0.2128	142	55	1.0801	4.7930	0.2254
93	37	0.9998	4.8938	0.2043	143	55	1.1293	4.8938	0.2308
92	37	0.9780	4.9986	0.1957	144	55	1.1802	4.9986	0.2361
91	36	1.0249	4.9087	0.2088	145	56	1.1172	4.9087	0.2276
90	35	1.0752	4.8382	0.2222	146	57	1.0604	4.8382	0.2192
89	35	1.0652	4.9898	0.2135	147	57	1.1202	4.9898	0.2245
88	35	1.0532	5.1492	0.2045	148	57	1.1829	5.1492	0.2297
87	34	1.0945	5.0114	0.2184	149	58	1.1099	5.0114	0.2215
86	33	1.1339	4.8756	0.2326	150	59	1.0401	4.8756	0.2133
85	33	1.1210	5.0151	0.2235	151	59	1.0960	5.0151	0.2185
84	33	1.1080	5.1708	0.2143	152	59	1.1566	5.1708	0.2237
83	33	1.0947	5.3449	0.2048	153	59	1.2227	5.3449	0.2288
82	33	1.0665	5.4659	0.1951	154	59	1.2778	5.4659	0.2338
81	32	1.1248	5.3592	0.2099	155	60	1.2101	5.3592	0.2258
80	33	1.0229	5.8451	0.1750	156	59	1.4238	5.8451	0.2436
79	31	1.1504	5.3461	0.2152	157	61	1.1918	5.3461	0.2229
78	31	1.1440	5.5771	0.2051	158	61	1.2707	5.5771	0.2278
77	30	1.2168	5.5116	0.2208	159	62	1.2132	5.5116	0.2201
76	30	1.1706	5.5601	0.2105	160	62	1.2510	5.5601	0.2250

for thermal neutron-induced fission of actinides. Therefore, the expression of the phenomenological parameter α can be presumed as:

$$\alpha = a_{L, H} + a_k(A - A_i^p)^2, \quad (24a)$$

$$(Z_f - 54) \leq Z \leq Z_f/2 \text{ or } Z_f/2 \leq Z \leq 54,$$

and

$$\alpha = \delta_{L, H}bZ + c_{L, H} + \delta_{L, H}kA, \quad (24b)$$

$$Z \leq (Z_f - 54) \text{ or } Z \geq 54.$$

Where $A_{H0}^p=132$, $A_{L0}^p = A_f - A_{H0}^p$ and $\delta_L=-1$, $\delta_H=1$. If the deformation parameter β is assumed as a smooth

function of A and Z for a large amount of the primary fragments, so the coefficients in Eqs. (24a) and (24b) can be derived as:

$$\begin{cases} a_k = k/16 \\ a_L = -(Z_f - 54)b + c_L - (A_f - 136)k \\ a_H = 54b + c_H + 136k \\ c_H = -Z_fb - A_fk + c_L. \end{cases} \quad (25)$$

Thus, there are only three adjustable free coefficients $\{k, b, c_L\}$ for describing the general rule of the deformation parameter β of the Most Probable Primary Fragment Pairs. Furthermore, this rule is extended to de-

TABLE IV. The properties of the Most Probable Primary Fragment Pairs for $^{239}\text{Pu}(n_{th}, f)$ reaction.

A_{L0}	Z_{L0}	β_{L0}	α_{L0}	I_{L0}	A_{H0}	Z_{H0}	β_{H0}	α_{H0}	I_{H0}
120	47	1.3458	6.2112	0.2167	120	47	1.3458	6.2112	0.2167
119	47	1.2634	6.0140	0.2101	121	47	1.3420	6.0140	0.2231
118	45	1.2931	5.4494	0.2373	122	49	1.0720	5.4494	0.1967
117	46	1.1439	5.3533	0.2137	123	48	1.1751	5.3533	0.2195
116	45	1.1684	5.2129	0.2241	124	49	1.0930	5.2129	0.2097
115	45	1.0707	4.9252	0.2174	125	49	1.0638	4.9252	0.2160
114	45	1.0014	4.7567	0.2105	126	49	1.0570	4.7567	0.2222
113	45	0.9579	4.7061	0.2035	127	49	1.0746	4.7061	0.2283
112	45	0.9147	4.6567	0.1964	128	49	1.0914	4.6567	0.2344
111	45	0.8628	4.5606	0.1892	129	49	1.0960	4.5606	0.2403
110	45	0.8236	4.5300	0.1818	130	49	1.1151	4.5300	0.2462
109	44	0.8661	4.4956	0.1927	131	50	1.0639	4.4956	0.2366
108	45	0.7658	4.5945	0.1667	132	49	1.1834	4.5945	0.2576
107	43	0.8834	4.5011	0.1963	133	51	1.0491	4.5011	0.2331
106	43	0.8615	4.5661	0.1887	134	51	1.0904	4.5661	0.2388
105	42	0.9075	4.5377	0.2000	135	52	1.0420	4.5377	0.2296
104	42	0.8851	4.6024	0.1923	136	52	1.0829	4.6024	0.2353
103	41	0.9401	4.6111	0.2039	137	53	1.0434	4.6111	0.2263
102	41	0.9134	4.6585	0.1961	138	53	1.0802	4.6585	0.2319
101	41	0.9094	4.8341	0.1881	139	53	1.1477	4.8341	0.2374
100	41	0.8943	4.9685	0.1800	140	53	1.2066	4.9685	0.2429
99	40	0.9468	4.9332	0.1919	141	54	1.1546	4.9332	0.2340
98	39	0.9980	4.8902	0.2041	142	55	1.1020	4.8902	0.2254
97	39	0.9818	5.0122	0.1959	143	55	1.1567	5.0122	0.2308
96	39	0.9639	5.1406	0.1875	144	55	1.2138	5.1406	0.2361
95	38	1.0098	5.0489	0.2000	145	56	1.1491	5.0489	0.2276
94	37	1.0646	5.0038	0.2128	146	57	1.0967	5.0038	0.2192
93	37	1.0380	5.0805	0.2043	147	57	1.1405	5.0805	0.2245
92	37	1.0326	5.2778	0.1957	148	57	1.2125	5.2778	0.2297
91	36	1.0708	5.1287	0.2088	149	58	1.1359	5.1287	0.2215
90	35	1.1234	5.0553	0.2222	150	59	1.0785	5.0553	0.2133
89	35	1.1089	5.1943	0.2135	151	59	1.1352	5.1943	0.2185
88	35	1.0992	5.3738	0.2045	152	59	1.2020	5.3738	0.2237
87	34	1.1536	5.2821	0.2184	153	60	1.1393	5.2821	0.2157
86	34	1.1251	5.3757	0.2093	154	60	1.1868	5.3757	0.2208
85	34	1.1045	5.5223	0.2000	155	60	1.2470	5.5223	0.2258
84	33	1.1650	5.4366	0.2143	156	61	1.1849	5.4366	0.2179
83	33	1.1594	5.6605	0.2048	157	61	1.2619	5.6605	0.2229
82	33	1.1391	5.8380	0.1951	158	61	1.3302	5.8380	0.2278
81	32	1.1577	5.5159	0.2099	159	62	1.2142	5.5159	0.2201
80	33	1.0730	6.1315	0.1750	160	61	1.4562	6.1315	0.2375

scribe the deformation parameters of arbitrary primary fragments for $^{235}\text{U}(n_{th}, f)$ and $^{239}\text{Pu}(n_{th}, f)$ reactions.

IV. RESULT AND ANALYSIS

A. Average total kinetic energy

Based on the DSM introduced in the last sections II and III, the explicit average total kinetic energy distribution $\overline{TK\overline{E}}(A)$ is expressed as Eq. (21), and the quadrupole deformation parameter of the arbitrary primary fragments is also expressed as Eqs. (23)-(25). Thus, the root-mean-square deviation σ can be expressed

as:

$$\sigma = \sqrt{\frac{1}{\sum_j} \sum_j [\overline{TK\overline{E}}_{th}(A_j) - \overline{TK\overline{E}}_{exp}(A_j)]^2}, \quad (26)$$

which is adopted to determine the agreement between the theoretical calculations and the experimental data. Where the $\overline{TK\overline{E}}_{th}$ and $\overline{TK\overline{E}}_{exp}$ denote the theoretical values and experimental data with small relative errors [31, 32] are selected to obtain a set of the optimal parameters $\{k, b, c_L\}$ listed in Table V both for $^{235}\text{U}(n_{th}, f)$ and $^{239}\text{Pu}(n_{th}, f)$ reactions.

Figs. 6 and 7 show the comparisons of the calculated average total kinetic energies $\overline{TK\overline{E}}(A)$ with the measurements for $^{235}\text{U}(n_{th}, f)$ and $^{239}\text{Pu}(n_{th}, f)$ reactions, respectively. The experimental data are derived from Refs.

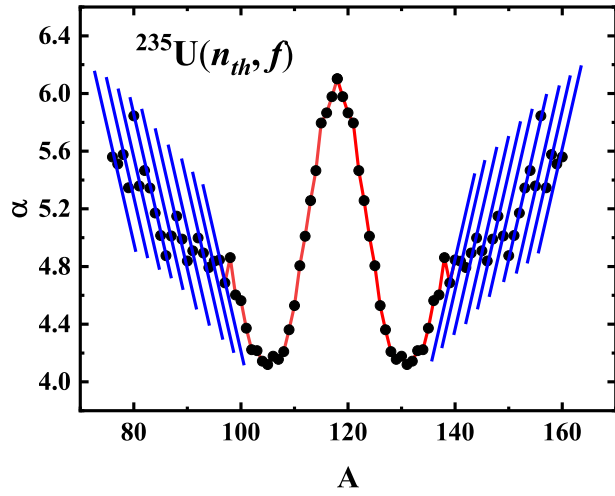


FIG. 4. (Color online) The relationship between phenomenological parameters α and the mass number A for $^{235}\text{U}(n_{th}, f)$ reaction. The red and blue lines show the results of Eqs. (24a)-(25).

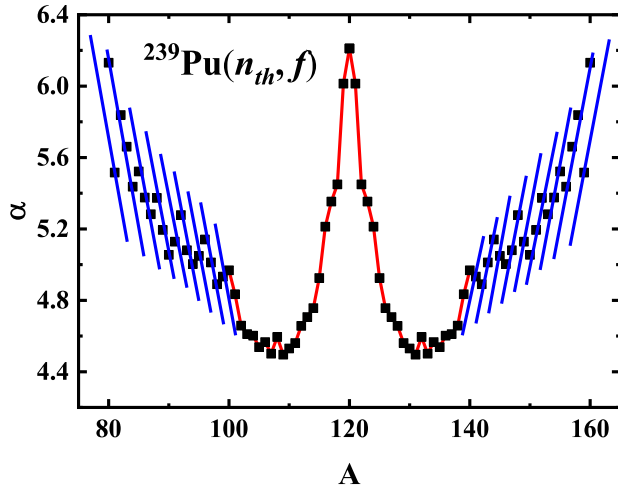


FIG. 5. (Color online) The relationship between phenomenological parameters α and the mass number A for $^{239}\text{Pu}(n_{th}, f)$ reaction.

[31, 45–52]. The red line and green lines denote the calculated results of this work and Pre-Scission Configuration (PSC) approach [24], respectively. It can be seen that all of the calculated results are reasonable, with their root-mean-square deviations $\sigma_{\overline{TKE}}$ listed in Table VI. It is obvious that the results of this work is slightly superior to those of the PSC approach.

TABLE V. The optimal coefficients of the deformation parameter (no units).

k	b	c_L
0.1943	-0.4151	7.7924

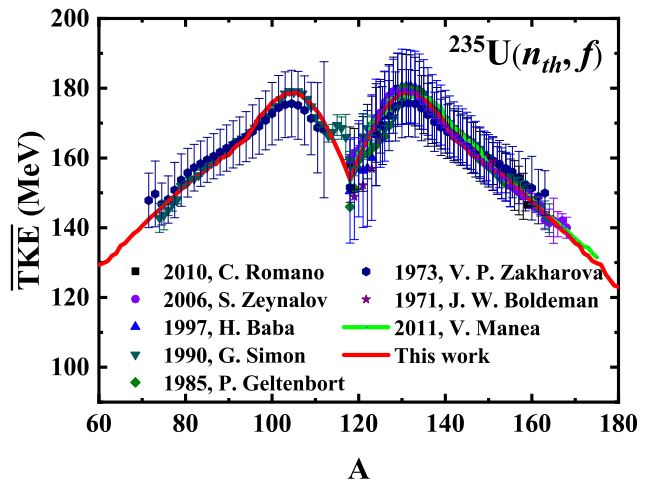


FIG. 6. (Color online) Comparisons of the calculated average total kinetic energy $\overline{TKE}(A)$ with the measurements for $^{235}\text{U}(n_{th}, f)$ reaction. The experimental data are derived from Refs. [31, 45–49]. The red line and green lines denote the theoretical results of this work and PSC approach [24], respectively.

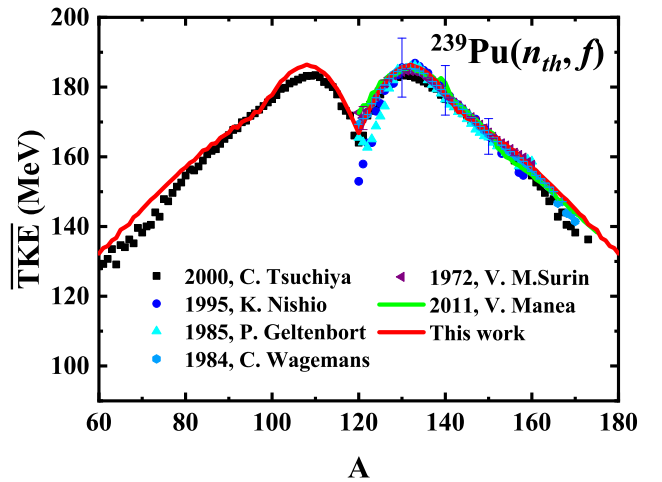


FIG. 7. (Color online) Comparisons of the calculated average total kinetic energy $\overline{TKE}(A)$ with the measurements for $^{239}\text{Pu}(n_{th}, f)$ reaction. The experimental data are derived from Refs. [32, 47, 50–52].

TABLE VI. Root-mean-square deviations σ of the different models.

Fission system	$\sigma_{\overline{TKE}}$ (MeV)	$\sigma_{\overline{KE}}$ (MeV)	Models
$^{235}\text{U}(n_{th}, f)$	1.32	1.26	DSM
	2.01	/	PSC [24]
	/	1.73	GEF [53]
$^{239}\text{Pu}(n_{th}, f)$	2.11	1.09	DSM
	2.95	/	PSC [24]
	/	2.22	GEF [53]

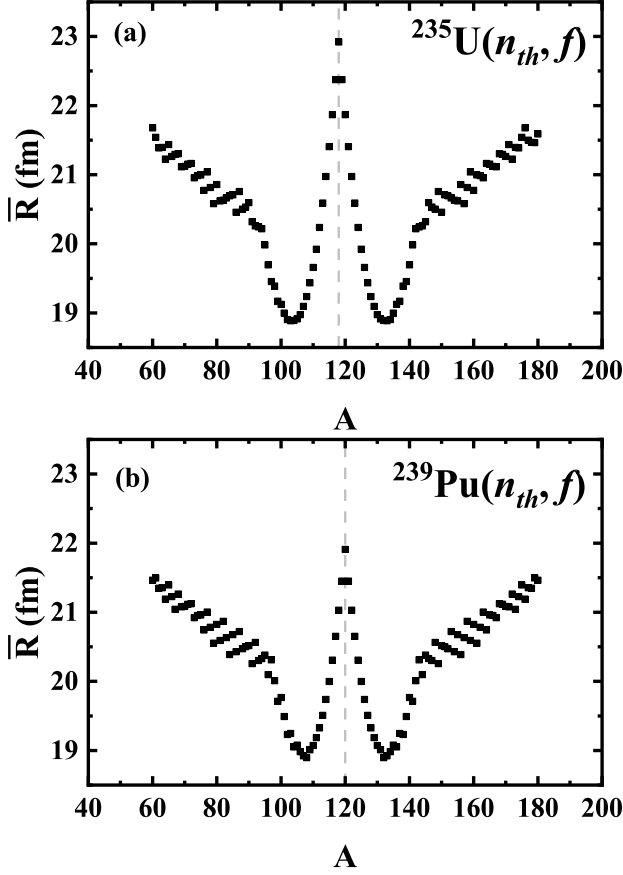


FIG. 8. (Color online) The average distance \bar{R} versus mass number A for $^{235}\text{U}(n_{th}, f)$ reaction (a) and $^{239}\text{Pu}(n_{th}, f)$ reaction (b).

From Eq. (18), it can be seen that the distance R between the mass centers of the complementary light and heavy primary fragments is critical. In terms of Eq. (6), the average distance \bar{R} between the mass centers of complementary primary fragments can also be rewritten as a function of mass number A :

$$\bar{R}(A) = \frac{1}{\sum_k} \sum_k R(A_{L0}(j), Z_{L0}(j, k), \beta_{L0}(j, k); A_{H0}(j), Z_{H0}(j, k), \beta_{H0}(j, k)). \quad (27)$$

Fig. 8 shows the average distance \bar{R} versus the mass number A for $^{235}\text{U}(n_{th}, f)$ reaction (a) and $^{239}\text{Pu}(n_{th}, f)$ reaction (b), from which it can be seen that there are one peak at the symmetric fission point $A_f/2$ and two valleys at $A = 132$ and $A = A_f - 132$ positions, with the peak value for $^{235}\text{U}(n_{th}, f)$ reaction being higher than that for $^{239}\text{Pu}(n_{th}, f)$ reaction. It implies that the TKE at the symmetric fission point $A_f/2$ of $^{235}\text{U}(n_{th}, f)$ reaction is smaller than that of $^{239}\text{Pu}(n_{th}, f)$ reaction, as shown in Figs. 6 and 7.

Fig. 9 shows the deformation at the scission moment and half-life in the ground state of the possible isobar

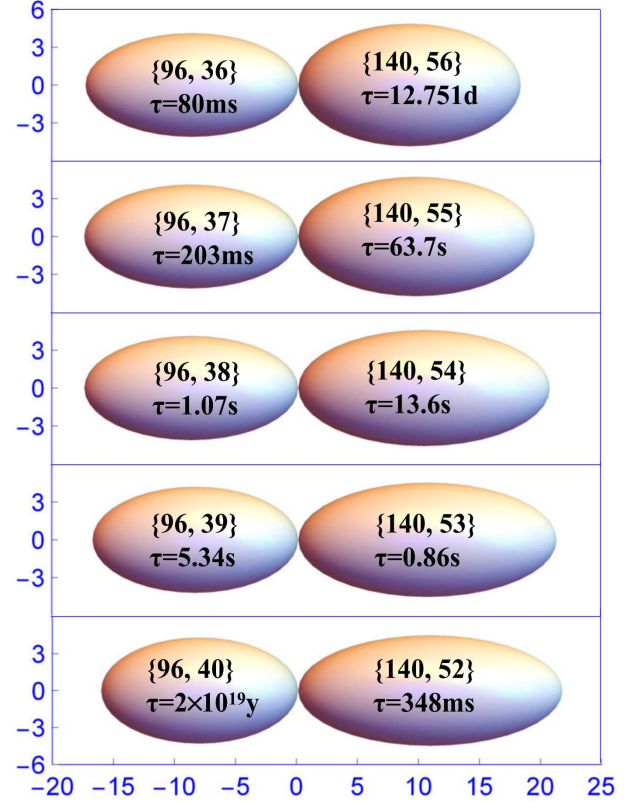


FIG. 9. (Color online) The deformation at the scission moment and half-life in the ground state of the possible isobar pairs of $A_{L0} = 96$ and $A_{H0} = 140$ for $^{235}\text{U}(n_{th}, f)$ reaction.

pairs of $A_{L0} = 96$ and $A_{H0} = 140$ for $^{235}\text{U}(n_{th}, f)$ reaction. And Fig. 10 shows the deformation at the scission moment and half-life in the ground state of the possible isobar pairs of $A_{L0} = 100$ and $A_{H0} = 140$ for $^{239}\text{Pu}(n_{th}, f)$ reaction. Obviously, the isobar pair with the smallest half-life in the ground state holds the smallest deformation at the scission moment. This implies that the kinetic energy of the primary fragments can be manifested by some properties of their ground state. Several properties of the Most Probable Primary Fragment Pairs, such as the quadrupole deformation parameter β_i , phenomenological parameter α_i and the isospin asymmetry degree I_i , are listed in Tables III and IV for $^{235}\text{U}(n_{th}, f)$ and $^{239}\text{Pu}(n_{th}, f)$ reactions, respectively.

B. Average kinetic energy

The subjects of the total kinetic energy TKE are the complementary primary fragment pairs. However, the energy allocation of light and heavy primary fragments is different. In terms of the conservations of momentum

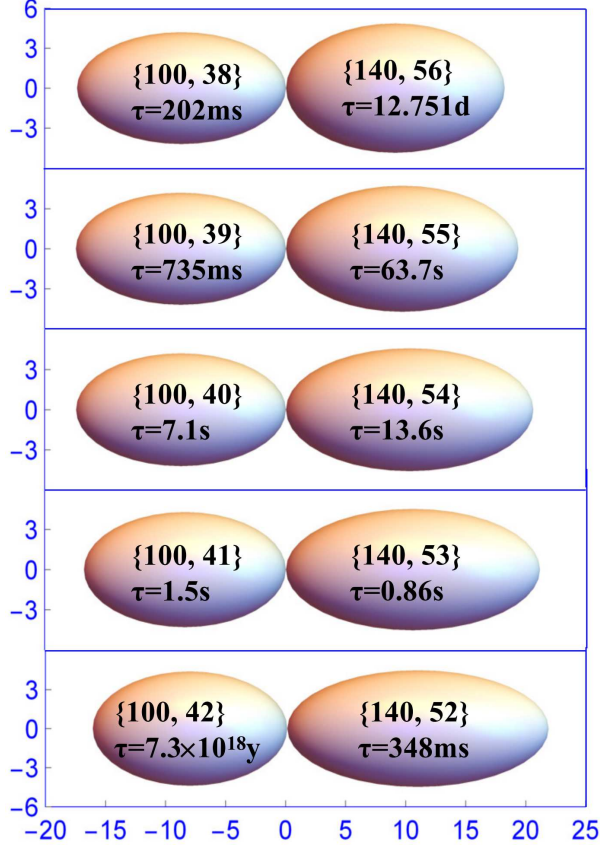


FIG. 10. (Color online) The deformation at the scission moment and half-life in the ground state of the possible isobar pairs of $A_{L0} = 100$ and $A_{H0} = 140$ for $^{239}\text{Pu}(n_{th}, f)$ reaction.

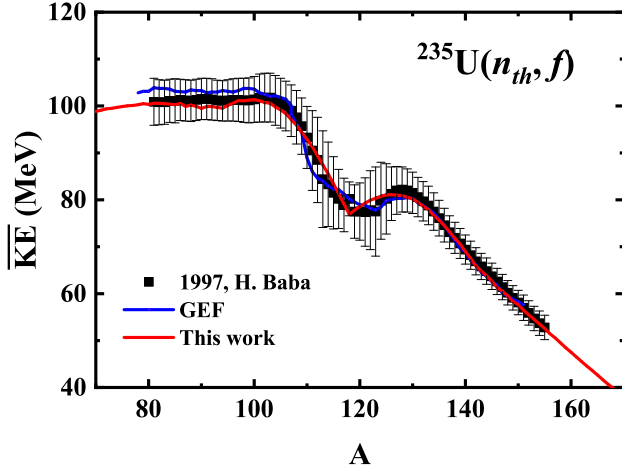


FIG. 11. (Color online) Comparisons of the average kinetic energy $\overline{KE}(A)$ with the measurements and model calculations for $^{235}\text{U}(n_{th}, f)$ reaction. The experimental data are derived from Ref. [31]. The red and blue lines denote the results of this work and GEF model [53], respectively.

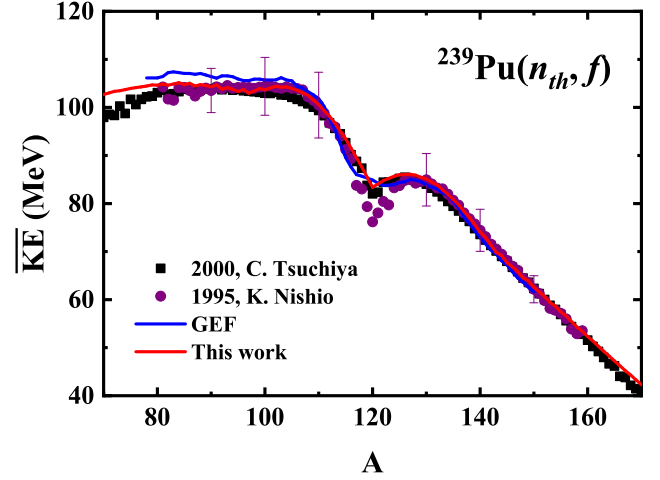


FIG. 12. (Color online) Comparisons of the average kinetic energy $\overline{KE}(A)$ with the measurements and model calculations for $^{239}\text{Pu}(n_{th}, f)$ reaction. The experimental data are derived from Refs. [32, 51].

and kinetic energy as follows,

$$\begin{cases} m_{L0}v_{L0} = m_{H0}v_{H0} \\ \frac{1}{2}m_{L0}v_{L0}^2 + \frac{1}{2}m_{H0}v_{H0}^2 = TKE, \end{cases} \quad (28)$$

the kinetic energy of the heavy primary fragment KE_{H0} is defined as:

$$\begin{aligned} KE_{H0} &= \frac{1}{2}m_{H0}v_{H0}^2 \\ &= \frac{m_{L0}}{m_{L0} + m_{H0}}TKE \\ &\approx \frac{A_{L0}}{A_f}TKE. \end{aligned} \quad (29)$$

And the kinetic energy of the light primary fragment KE_{L0} can be easily written as:

$$\begin{aligned} KE_{L0} &= TKE - KE_{H0} \\ &\approx \frac{A_{H0}}{A_f}TKE. \end{aligned} \quad (30)$$

Thus, the average kinetic energy distribution $\overline{KE}(A)$ can be expressed as:

$$\overline{KE}(A) = \frac{1}{\sum_k} \sum_k KE(A_{L0}(j), Z_{L0}(j, k); A_{H0}(j), Z_{H0}(j, k)), \quad (31)$$

or

$$\overline{KE}(A) = \frac{A_f - A}{A_f}TKE(A). \quad (32)$$

Further, it can be found that the results of Eqs. (31) and (32) are roughly equal. Evidently, Eq. (32) simple and convenient, is used in this paper.

Figs. 11 and 12 show the comparisons of the calculated and measured $\overline{KE}(A)$ for $^{235}\text{U}(n_{th}, f)$ and $^{239}\text{Pu}(n_{th}, f)$, respectively. The red and blue lines denote the results of this work and GEF model [53], respectively. And the root-mean-square deviations $\sigma_{\overline{KE}}$ of this work and GEF are listed in Table VI. From Figs. 11 and 12 and Table VI, it can be seen that all of the calculated results of this paper is reasonable and slightly superior to those of GEF model.

V. CONCLUSION

Based on the dinuclear concept, if it is assumed that the fissile nucleus elongates along an coaxis and attains the scission point, the kinetic energy of the complementary primary fragment pairs is mainly provided by the Coulomb repulsion. After performing strictly the six-dimensional integral and omitting the higher order terms, the compact expression of the Coulomb repulsion is explicitly obtained. In terms of the statistical properties of the abundant experimental total kinetic energy distributions, mass and charge distributions, and our previous theoretical results, some special quantities (such as mass numbers $A = 132$ and 140 , charge number $Z = 54$, and

symmetrical fission point $\{A_f/2, Z_f/2\}$) are used to derive the phenomenological expression of the deformation parameters of the different primary fragments at the scission moment. And a set of optimal coefficients $\{k, b, c_L\}$ of the deformation parameters of arbitrary complementary fragments is obtained both for $^{235}\text{Pu}(n_{th}, f)$ and $^{239}\text{Pu}(n_{th}, f)$ reactions. The calculated results concurrently agree well with the measured total kinetic energy distributions $\overline{TKE}(A)$ and experimental kinetic energy distributions $\overline{KE}(A)$, and are also slightly better than the previous theoretical ones.

However, the DSM model omits the rotational energy, which largely contributes to heavy-ion induced reactions due to the big angular momenta of the incident particle. In addition, nuclear charge densities have an exponential tails rather than a sharp surface, so DSM ignores the attractive nuclear force at the scission moment because of the super coaxial deformation. Due to the fact that the DSM model can provide enough trust for the $\overline{TKE}(A)$ and $\overline{KE}(A)$, the feasibility is expected to extend the arbitrary incident energies and/or other fissile systems.

ACKNOWLEDGMENTS

We appreciate the valuable suggestions of our colleagues Drs. Ning Wang, Li Ou and Min Liu.

-
- [1] O. Hahn and F. Strassmann, *Naturwissenschaften* **27**, 11 (1939).
- [2] C. Schmitt, K.-H. Schmidt, and B. Jurado, *Phys. Rev. C* **98**, 044608 (2018).
- [3] R. Vogt, J. Randrup, J. Pruet, and W. Younes, *Phys. Rev. C* **80**, 044611 (2009).
- [4] F.-J. Hamsch, S. Oberstedt, A. Al-Adili, *et al.*, *Nucl. Data Sheets* **119**, 38 (2014).
- [5] D. Neudecker, T. N. Taddeucci, R. C. Haight, *et al.*, *Nucl. Data Sheets* **131**, 289 (2016).
- [6] M. E. Gooden, C. W. Arnold, J. A. Becker, *et al.*, *Nucl. Data Sheets* **131**, 319 (2016).
- [7] S. Goriely, J.-F. Sida, J.-F. Lemaître, *et al.*, *Phys. Rev. Lett.* **111**, 242502 (2013).
- [8] M. Eichler, A. Arcones, A. Kelic, *et al.*, *The Astrophysical Journal* **808**, 1 (2015).
- [9] D. Higgins, U. Greife, F. Tovesson, *et al.*, *Phys. Rev. C* **101**, 014601 (2020).
- [10] G. Scamps and C. Simenel, *Nature* **564**, 382 (2018).
- [11] N. Schunck and L. M. Robledo, *Rep. Prog. Phys.* **79**, 116301 (2016).
- [12] D. Regnier, M. Verrire, N. Dubray, and N. Schunck, *Comput. Phys. Commun.* **200**, 350 (2016).
- [13] J. Zhao, T. Nikšić, D. Vretenar, and Sh. G. Zhou, *Phys. Rev. C* **99**, 014618 (2019).
- [14] J.-F. Lemaître, S. Goriely, S. Hilaire, and J.-L. Sida, *Phys. Rev. C* **99**, 034612 (2019).
- [15] M. T. Mustonen, C. N. Gilbreth, Y. Alhassid, and G. F. Bertsch, *Phys. Rev. C* **98**, 034317 (2018).
- [16] D. E. Ward, B. G. Carlsson, T. Døssing, *et al.*, *Phys. Rev. C* **95**, 024618 (2017).
- [17] P. Goddard, P. Stevenson, and A. Rios, *Phys. Rev. C* **92**, 054610 (2015).
- [18] D. A. Brown, M. B. Chadwick, R. Capote, *et al.*, *Nuclear Data Sheets* **148**, 1 (2018).
- [19] <https://www.oecd-nea.org/dbdata/jeff/jeff33/index.html>.
- [20] <https://www-nds.iaea.org/public/download-endf/JENDL-4.0u2-2>
- [21] Z. G. Ge, Z. X. Zhao, H. H. Xia, *et al.*, *J. Korean Phys. Soc.* **59**, 1052 (2011).
- [22] Z. M. Niu and H. Z. Liang, *Phys. Lett. B* **778**, 48 (2018).
- [23] Z. A. Wang, J. Ch. Pei, and Y. Qiang, *Phys. Rev. Lett.* **123**, 122501 (2019).
- [24] V. Manea and Anabella. Tudora, *Annals of Nuclear Energy* **38**, 72 (2011).
- [25] D. G. Madland, *Nucl. Phys. A* **772**, 113 (2006).
- [26] V. Yu. Denisov and N. A. Pilipenko, *Phys. Rev. C* **76**, 014602 (2007).
- [27] B. C. Carlson and G. S. Rushbrooke, *Proc. Cambridge Philos. Soc* **46**, 626 (1950).
- [28] N. W. ang T. Li, *Phys. Rev. C* **88**, 011301 (2013).
- [29] M. Wang, G. Audi, F. G. Kondev, *et al.*, *Chinese Physics C* **41**, 139 (2017).
- [30] <https://www-nds.iaea.org/relnsd/vcharthtml/VChartHTML.html>.
- [31] H. Baba, T. Saito, N. Takahashi, *et al.*, *Journal of Nuclear Science and Technology* **34**, 871 (1997).
- [32] C. Tsuchiya, Y. Nakagome, H. Yamana, *et al.*, *Journal of Nuclear Science and Technology* **37**, 941 (2000).
- [33] H. Thierens, E. Jacobs, P. D'hondt, *et al.*, *Phys. Rev. C* **29**, 498 (1984).
- [34] X. J. Sun, Ch. G. Yu, and N. Wang, *Phys. Rev. C* **85**, 014613 (2012).
- [35] X. J. Sun, Ch. H. Pan, Ch. G. Yu, *et al.*,

- Communication in Theoretical Physics **62**, 711 (2014).
- [36] X. J. Sun, Ch. G. Yu, N. Wang, *et al.*, *Chinese Physics C* **39**, 014102 (2015).
- [37] M. Asghar, F. Caiüicoli, P. Perrin, *et al.*, *Nucl. Phys. A* **311**, 413 (1978).
- [38] M. Asghar, F. Caiüicoli, B. Leroux, *et al.*, *Nucl. Phys. A* **368**, 328 (1981).
- [39] C. Romano, Y. Danon, R. Block, *et al.*, *Phys. Rev. C* **81**, 014607 (2010).
- [40] C. Wagemans, E. Allaert, F. Caiüicoli, *et al.*, *Nucl. Phys. A* **369**, 1 (1981).
- [41] M. Asghar, F. Caiüicoli, P. Perrin, *et al.*, *Nucl. Phys. A* **334**, 327 (1980).
- [42] W. Reisdorf, J. P. Unik, H. C. Griffin, and L. E. Glendenin, *Nucl. Phys. A* **177**, 337 (1971).
- [43] H. Naik, S. P. Dange, R. J. Singh, and S. B. Manohar, *Nucl. Phys. A* **612**, 143 (1997).
- [44] H. Naik, R. J. Singh, and R. H. Lyer, *Journal of Physics G: Nuclear and Particle Physics* **30**, 217 (2004).
- [45] G. Simon, J. Trochon, F. Brisard, *et al.*, *Nuclear Instruments and Methods in Physics Research Section A: Accelerators, Detectors and Related Equipment* **538**, 103 (2005).
- [46] S. Zeynalov, W. Furman, and F. J. Hamsch, *Proceedings of the 13th International Seminar on Interaction of Neutrons with Matter*, 199 (1997).
- [47] P. Geltenbort, F. Gönnerwein, and A. Oed, *Radiation Effects* **93**, 57 (1986).
- [48] V. P. Zakharova, D. K. Ryazanov, B. G. Basova, *et al.*, *Yadern. Fiz.* **18**, 710 (1973).
- [49] J. W. Boldeman, A. R. D. L. Musgrove, and R. L. Walsh, *Australian Journal of Physics* **24**, 821 (1971).
- [50] C. Wagemans, E. Allaert, A. Deruytter, *et al.*, *Phys. Rev. C* **30**, 218 (1984).
- [51] K. Nishio, Y. Nakagome, I. Kanno, *et al.*, *Journal of Nuclear Science and Technology* **32**, 404 (1995).
- [52] V. M. Surin, A. I. Sergachev, N. I. Rezchikov, *et al.*, *Yadern. Fiz.* **14**, 935 (1971).
- [53] K.-H. Schmidt, B. Jurado, C. Amouroux, and C. Schmitt, *Nuclear Data Sheets* **131**, 107 (2016).